Thermal radiation dynamics in two parallel plates: The role of near field

S. A. Dyakov,[*] J. Dai, and M. Yan

Department of Materials and Nano Physics, School of Information and Communication Technology, Royal Institute of Technology,
Electrum 229, 16440 Kista, Sweden

M. Qiu[†]

State Key Laboratory of Modern Optical Instrumentation, Department of Optical Engineering, Zhejiang University, 310027 Hangzhou, China
and Department of Materials and Nano Physics, School of Information and Communication Technology, Royal Institute of Technology,
Electrum 229, 16440 Kista, Sweden

The temperature dynamics of the radiative heat propagation in a multilayer structure is theoretically treated with a formalism combining the scattering matrix and Green's-functions methods. The time evolution of the temperature of parallel plates of silicon carbide in vacuum is simulated for different interplate distances and thicknesses of plates. The characteristic radiative heat exchange time and temperature of the plates at stationary state are determined from the time evolutions. The threshold interplate distance which separates heating and cooling regimes for the sink plate is found. We show that the variation of the interplate distance allows us to control the relaxation processes in the system of absorber and emitter.

I. INTRODUCTION

The character of the radiative heat transfer from one body to another strongly depends on the shape and the distance between them. The Stefan-Boltzmann law predicts the power of the radiative heat exchange between two objects as $\sigma(T_2^4 - T_1^4)$, where σ is the Stefan-Bolzmann constant and $T_{1,2}$ are the temperatures of objects. The applicability of this law is limited by the following constraints. The first constraint is that the Stefan-Bolzmann law is related only to blackbodies. The second constraint is that the distance between the heat source and sink, d, must be large enough compared to the characteristic wavelength of thermal emission. At the same time, it was shown in many publications that when the distance between the objects is much smaller than the characteristic wavelength of thermal emission the heat transfer intensity can be sufficiently enhanced [1,2]. The enhancement of radiative heat transfer intensity in the near field is due to coupling of evanescent photons which correspond to the surface states such as plasmon polaritons and phonon polaritons. In this case, thermal radiation between two bodies exceeds that between two blackbodies in the far field by orders of magnitude [3]. Such drastically enhanced heat transfer phenomena can immediately lead to design of microstructures and nanostructures with artificially engineered thermal conductivities for applications where effective and efficient heat management is necessary. The potential applications of near-field effects include thermovoltaics [4–6], thermal emission control [7–12], heat-assisted magnetic recording [13], etc. There are series of theoretical studies in recent years concerning the near-field-mediated heat transfer between two bodies of various geometries (see, for example, [3,14–35]). Experimentally, enhancement of heat exchange between two bodies in the near-field limit has been demonstrated for plane-plane and sphere-plane geometry.

The previous theoretical and experimental efforts focus almost exclusively on steady-state heat transfer problems where heat source, sink, and boundary conditions are defined irrespective to time. In reality, systems are subject to perturbations; therefore the transient heat transfer plays an important role for the systems' overall thermal performance. Even for many steady-state heat transfer problems, it is important to know how long it takes for a system to achieve stationary state after its heat source is turned on. Intuitively we understand that a decrease in distance between a heat source and sink leads to an enhancement of the radiative heat transfer coefficient and, therefore, to a shortening of time for the system to reach stationary state. However, a more accurate assessment of the heat transfer dynamics should consider complications such as the temperature-dependent mass heat capacity, density, and dielectric permittivity of materials, which are all time-varying parameters. There are very few theoretical studies addressing transient radiative heat exchange between bodies, with consideration of near-field tunneling.

Very recently, Messina *et al.* have simulated dynamics of heat transfer in systems of multiple dipoles [36]. They have shown that the time evolution of the temperatures in a three-body configuration strongly depends on the relative spatial localizations of the bodies. In [37] it is demonstrated theoretically that it is possible to exercise coherent control of the temperature in nanostructures by laser fields. The authors of [38] studied the radiative cooling of polar and metallic nanoparticles immersed in a thermal bath close to a partially reflecting surface and demonstrated the existence of an oscillating behavior for the thermal relaxation time with respect to the separation distance from the surface, an analog of Friedel oscillations in Fermi liquids. In [39] the temporal evolutions of metallic nanoparticles temperatures are analyzed and it is shown that it is possible to create a nanoscale temperature distribution in an ensemble of metallic nanoparticles with the aid of laser coherent control, without the

---

[*]sedyakov@kth.se
[†]minqiu@zju.edu.cn and min@kth.se

need for nanofabrication. Biehs and Agarwal have developed the dynamical quantum theory of heat transfer between two nanosystems and determined the heat transfer rate between two spherical nanoparticles [40]. In [41] the time evolution of temperatures of two different spheres was studied in the context of thermal rectification in near-field electromagnetic thermal transfer. Finally, in [42–45] the authors studied the radiative heat transfer occurring between arbitrary bodies in the nonequilibrium case where each body and the environment are at different temperatures.

In contrast to the aforementioned works, in the present paper we consider the phenomenon of transient radiative heat exchange between two parallel plates. Silicon carbide (SiC) is chosen for the plate material for its phonon resonances at long infrared range. Temperature-dependent material parameters are taken into account in our treatment, which has not been done before. Different aspects of radiative heat exchange dynamics when the distance between plates varies from 1 nm to 1 mm are studied. We simulated the time evolutions of temperature of the plates and determined the characteristic times it takes for a system to reach stationary state, $\tau_{\rm SS}$. It is found that the dependence of $\tau_{\rm SS}$ on the distance between plates and the thickness of plates is sufficiently different in near-field and far-field regimes. As a secondary objective, we show the algorithm of calculation of the radiative heat propagation inside an arbitrary multilayered structure.

In order to simulate the far-field and near-field radiative heat exchange between objects, we use the approaches of fluctuational electrodynamics [3,16]. The thermal radiation in the system of nonmagnetic layers is treated as an emission of chaotically oriented oscillating electric dipoles. The fluctuation-dissipation theorem relates the ensemble average of the spatial correlation function of the current density and the mean energy of Plank's oscillator. Then the Green's-function method in conjunction with scattering matrix formalism is used to find the thermal radiation fluxes at an arbitrary distance from the source. The advantage of this formalism is that it can be easily realized as an algorithm in programming languages for numerical computations.

The structure of the paper is as follows. In Sec. II of the paper we present the static study of the radiative heat exchange between plates of SiC and demonstrate the near-field coupling of the plates. In Sec. III A we present the theoretical model for the simulation of the dynamics of the heat transfer between parallel plates. In Sec. III B we simulate the transient dynamics of the radiative heat exchange between SiC plates. We consider the characteristic time it takes for plates to reach stationary state as well as the temperature of the plate in stationary state. In the Appendices we describe the theoretical approaches for investigation of the radiative heat propagation in a multilayer. In particular, we consider the scattering matrix formalism which is widely used for simulation of the propagation of plane waves and its analog for evanescent waves in a multilayer [46–48]. Further, we present the algorithm of calculation of the radiative heat exchange between the parallel layers.

II. STATIC STUDY OF RADIATIVE HEAT EXCHANGE

Before we describe the physical model for the near-field dynamics simulation, let us focus on the radiative heat
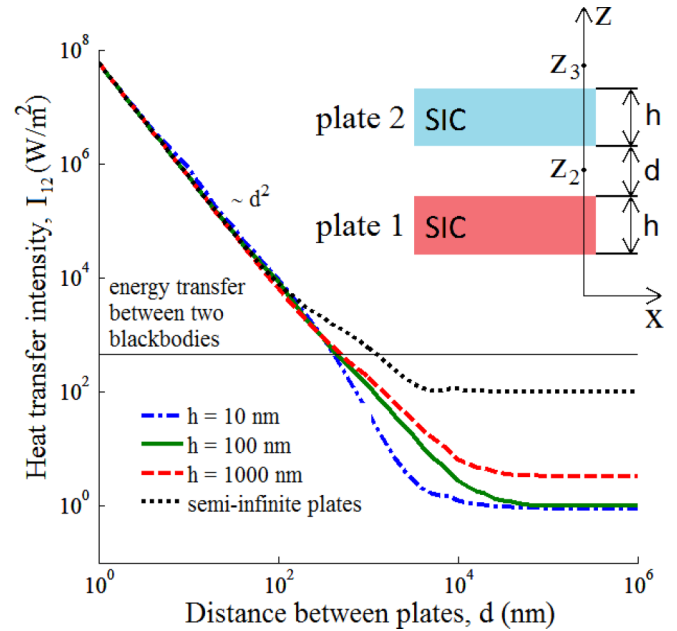

FIG. 1. (Color online) Intensity of the heat transfer from one SiC plate to another as a function of the distance between plates, d, calculated for different thicknesses of plates, h. Inset: Sketch of the structure.

exchange between objects without considering the temporal evolution of temperatures. We will need the results of this section later for an explanation of some of the effects in the transient radiative heat transfer. We consider a problem of heat exchange between two parallel plates of silicon carbide surrounded by vacuum (see inset in Fig. 1). The frequency-dependent relative permittivity of silicon carbide (SiC) is approximated by the oscillating Lorentz model:

$$\varepsilon_{\rm SiC} = \varepsilon_\infty \left[1 + \frac{\omega_L^2 - \omega_T^2}{\omega_T^2 - \omega^2 - i\gamma\omega} \right], \qquad (1)$$

and the parameters of oscillator are $\omega_L = 182.53$ THz, $\omega_T = 149.37$ THz, $\gamma = 0.8966$ THz, and $\varepsilon_\infty = 6.7$. The dispersion of the relative permittivity of SiC supports the surface phonon-polariton at the vacuum-SiC interface [3]. The horizontal asymptote of the surface phonon-polariton branch has the frequency of 178.4 THz. This means that if two plates of SiC are separated by a thin vacuum gap then the resonant penetration of photons from one plate to the other is possible.

The emission of thermal radiation is a quantum-mechanical process; however, it can be considered electrodynamically [3,19]. In this case, the thermal radiation is described as a fluctuating electromagnetic field generated by chaotic motion of charged particles inside the body. Mathematically, the corresponding current densities, $\vec{J}(\vec{r}')$, and electric and magnetic fields of thermal radiation, $\vec{E}(\vec{r})$ and $\vec{H}(\vec{r})$, are related via the Green's-function formalism:

$$\vec{E}(\vec{r},\omega) = i\omega \int_V G^E(\vec{r},\vec{r}',\omega)\vec{J}(\vec{r}',\omega)dV, \qquad (2a)$$

$$\vec{H}(\vec{r},\omega) = \int_V G^H(\vec{r},\vec{r}',\omega)\vec{J}(\vec{r}',\omega)dV, \qquad (2b)$$

where G^E and G^H are electric and magnetic dyadic Green's functions. The z projection of the time-averaged Poynting vector is expressed as [19]

$$S_z(z,\omega) = 2\mathrm{Re}[\langle E_x H_y^* - E_y H_x^* \rangle]. \qquad (3)$$

The fluctuation-dissipation theorem connects the ensemble average of the spatial correlation function of the current densities and the mean energy of Planck's oscillator at a given temperature $\Theta(\omega,T)$:

$$\langle J_\alpha(\vec{r},\omega) J_\beta(\vec{r}',\omega) \rangle = \frac{\omega \varepsilon_s''(\omega)}{\pi} \Theta(\omega,T)\delta(\vec{r}-\vec{r}')\delta(\omega-\omega')\delta_{\alpha\beta}, \qquad (4)$$

where α and β refer to orthogonal components x, y, or z. Taking into account Eqs. (2)–(4) we obtain the following expression for the spectral intensity of thermal radiation propagating along the z axis:

$$Q(\omega,z,T) = \frac{2\omega^2 \Theta(\omega,T)}{\pi c^2}$$
$$\times \mathrm{Re}\left[i\varepsilon_s'' \int_V \left(G_{x\alpha}^E G_{y\alpha}^{H*} - G_{y\alpha}^E G_{x\alpha}^{H*} \right) dV \right]. \qquad (5)$$

The intensity of thermal radiation is then calculated as an integral of spectral intensity:

$$I(z,T) = \int_0^\infty Q(\omega,z,T)d\omega. \qquad (6)$$

The dyadic Green's functions G^E and G^H are determined by the spatial distribution of dielectric permittivity in the sample and in the case of the layered structures can be found by the scattering matrix method (see Appendixes A and C).

Let us calculate the energy absorbed in plate 2 due to the thermal emission by plate 1 as a function of the distance between plates, d. We assume that the temperature of plate 1 is fixed at 300 K. Here, the temperature of the plate 2 is not specified as we do not consider the emission from plate 2. We calculate the intensity of the heat transfer from plate 1 to plate 2, I_{12}, as a difference between intensities of thermal radiation of plate 1, I_1, taken in the vacuum gap and in the upper semi-infinite vacuum: $I_{12} \equiv I_1(z_2) - I_1(z_3)$, where z_2 and z_3 are any z coordinates in the vacuum gap and in the upper semi-infinite vacuum correspondingly (see inset in Fig. 1).

The intensity of the heat transfer from plate 1 to plate 2, I_{12}, is shown in Fig. 1 as a function of gap size, d, calculated for different thickness of plates, h. It can be seen from Fig. 1 that for the gap size small enough compared with the wavelength of surface phonon resonance at the SiC-vacuum interface ($\approx 10\ \mu$m) the heat transfer intensity exceeds that of the blackbody by one to five orders of magnitude. This fact is well studied (see, for example, [3,17,49]) and is explained by coupling of the surface phonon-polariton resonances of the plates. Since the dispersion curves of these resonances are below the light line, the coupling takes place only for evanescent waves of thermal radiation. With decrease of d, the heat transfer intensity increases as $1/d^2$ for $d < 100$ nm. This dependence is in agreement with [50]. With increase of the separation distance d, coupling becomes weaker. For $d > 30\ \mu$m the function $I_{12}(d)$ is constant, which means that only propagating waves contribute to the heat exchange between
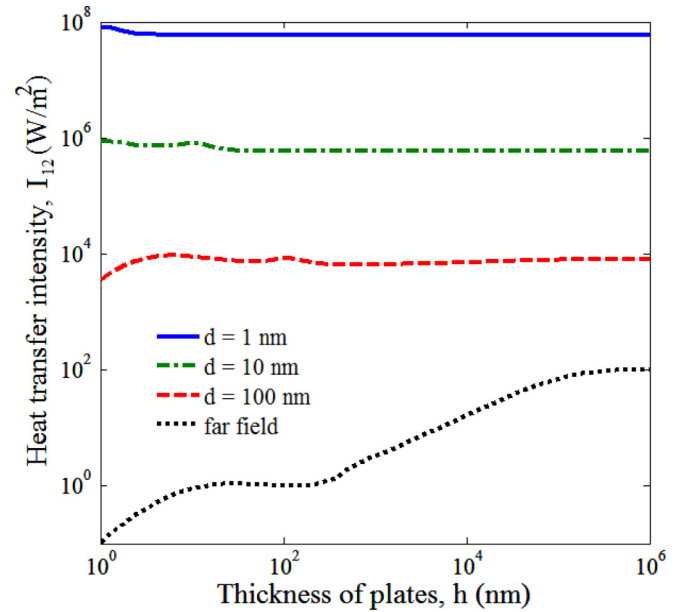

FIG. 2. (Color online) Intensity of the heat transfer from one SiC plate to another as a function of the thickness of plates, h, calculated for different distances between plates, d.

plates. This is in accordance with Wien's law, which states that the heat transfer intensity does not depend on the distance between objects. Based on the nature of the dependence $I(d)$, in Fig. 1 we can refer to the range of distances $d < 100$ nm as the near-field regime and the range $d > 30\mu$m as the far-field regime.

Figure 2 shows the heat transfer intensity as a function of the thickness of plates, h, calculated for the different distances d. One can see that in the near field I_{12} is almost independent of the thickness of plates (see curves $d = 1$, 10, and 100 nm in Fig. 2). Small oscillations of the heat transfer intensity for $h < d$ are due to the interference effect of guided surface phonon polariton waves in the plates. For $h > d$ these oscillations do not exist since the penetration depth of the evanescent waves of thermal radiation in SiC is very small [51]. Hence, the heat exchange between plates in the near field is determined by emission and absorption of the thin layers adjacent to the separation vacuum gap. In the far field, for small h the heat transfer intensity increases with increase of h since the thicker the emitting plate the more thermal energy it radiates. However, when the thickness of plates h is high enough compared to the thermal emission wavelength, the heat transfer intensity saturates to a constant value.

In order to demonstrate the coupling of the surface phonon polariton resonances between plates, let us calculate the spatial distribution of the electric field of vertically oriented oscillating electric dipoles located on the plane in the middle of plate 1. The method of dipole source terms is used for calculation of electric field and is described in Appendix B. We calculate the x component of the electric field for the angular frequency $\omega = 179.5$ THz and the x component of wave vector $k_x = 27.5k_0$, $k_0 = \omega/c$. The values of the parameters ω and k_x correspond to maximal surface phonon polariton coupling between 100-nm-thick plates separated by a 100-nm
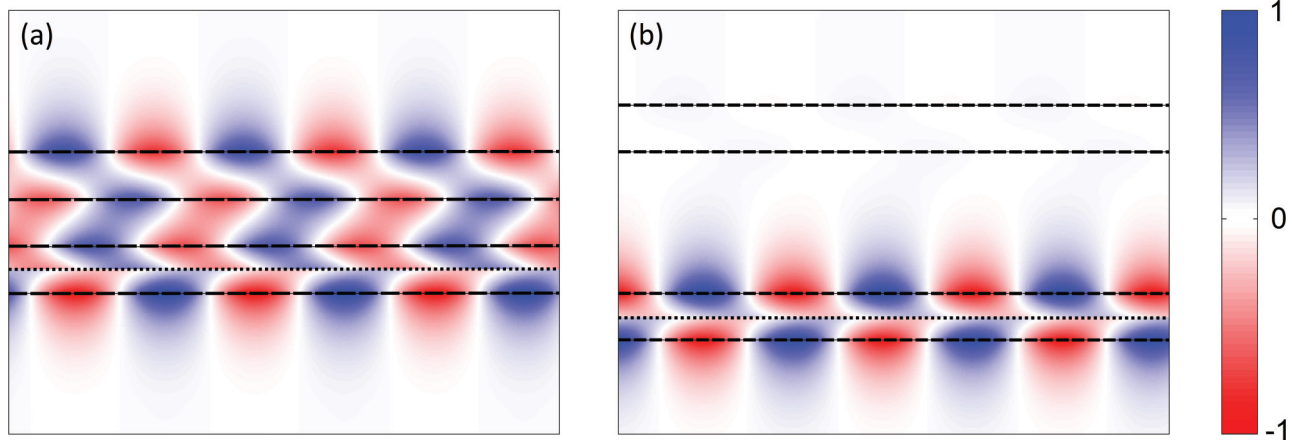
FIG. 3. (Color online) Spatial distributions of the x component of the electric field of a plane of vertically oriented oscillating dipoles located in the middle of the bottom SiC plate (dotted line). SiC plates are separated by a (a) 100-nm or (b) 300-nm vacuum gap. Parameters of calculation are the following: $\omega = 179.5$ THz; $k_x = 27.5k_0$, where k_0 is the wave vector in vacuum; and p polarization. Interfaces between layers are shown by dashed lines. The color scale on the right shows the calculated electric-field strength in arbitrary units.

vacuum gap. The maximal coupling implies the maximization of the integrands over k_x and ω in Eqs. (C1) and (C3) from Appendix C. The spatial distribution of the x component of the electric field is shown in Fig. 3(a). The field distribution clearly suggests the resonant coupling between surface phonon modes in two plates. For comparison, Fig. 3(b) shows the electric-field distribution calculated for the same ω and k_x but for $d = 300$ nm. Figure 3(b) demonstrates the absence of coupling of the surface phonon polariton resonances of the plates. For the other pair (ω, k_x) the coupling at $d = 300$ nm takes place; however, the efficiency of this coupling is lower than at $d = 100$ nm.

We have described some aspects of the radiative heat exchange between two SiC plates and have shown that the distance between plates determines the coupling efficiency of the surface phonon polariton modes. As expected from physical grounds, the higher the coupling efficiency the faster thermal power can be transferred from one plate to the other.

III. TRANSIENT DYNAMICS OF HEAT TRANSFER BETWEEN TWO PLATES OF SiC

A. Theoretical model

In this section we consider the dynamics of the radiative heat exchange between two parallel plates separated by a vacuum (see Fig. 4). We aim to calculate the temperatures of the bottom and top plates, T_1 and T_2, as a function of time, in the assumption that the temperature of a plate is changed only due to the radiative heat transfer from another plate. In particular, we exclude such ways of heat transfer as convection and conduction via heat carriers (phonons or electrons) since the plates are separated by a vacuum gap. In the below-described model, the thicknesses of plates d can be larger or smaller than the gap size h. The range of parameters d and h where the model is applicable is explicitly specified further in the paper. We assume that the temperatures $T_{1,2}$ can vary from 0 to 2650 K, the melting point of SiC. The temperature of the surroundings of the plates in Fig. 4 is 0 K.

We start by the energy balance equation of plate 2 in the time interval dt:

$$C_{v2}dT_2 = dE_{\text{in}} - dE_{\text{out}}, \quad (7)$$

where C_{v2} is the heat capacity at constant volume of plate 2, dE_{in} is the "incoming" energy of thermal radiation which is emitted by plate 1 during time interval dt and reaches plate 2, and dE_{out} is the "outgoing" energy which is dissipated in layer 2 during time interval dt due to the thermal radiation. Dividing Eq. (7) by mass $\rho_2 h_2 dS$ and time dt, we obtain

$$\frac{C_{v2}}{\rho_2 h_2 dS} \times \frac{dT_2}{dt} = \left(\frac{dE_{\text{in}}}{dt\,dS} - \frac{dE_{\text{out}}}{dt\,dS} \right) \times \frac{1}{\rho_2 h_2}, \quad (8)$$
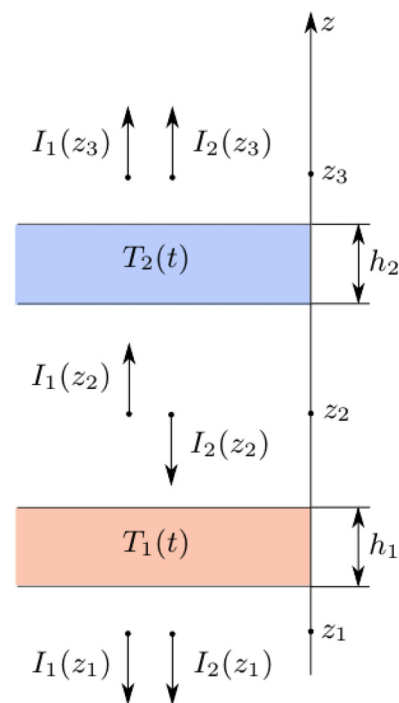

FIG. 4. (Color online) (a) Sketch of the two-plates structure and (b) thermal radiation fluxes from the top and bottom plates.

where ρ_2 is the density of the material of plate 2, dS is the elementary square, and h_2 is the thickness of plate 2. Taking into account that $c_{v2} \equiv C_{v2}/\rho_2 h_2 dS$ is the mass heat capacitance, we can write the energy balance equation in the following form:

$$\rho_2 c_{v2} h_2 \frac{dT_2(t)}{dt} = I_{\text{in}}(t) - I_{\text{out}}(t), \qquad (9)$$

where incoming intensity $I_{\text{in}} \equiv dE_{\text{in}}/dt\,dS$ and outgoing intensity $I_{\text{out}} \equiv dE_{\text{out}}/dt\,dS$ can be found by the method of oscillating dipoles and the fluctuation dissipation theorem (see Appendix C).

Let us consider the intensities of the heat propagation at coordinates z_1, z_2, and z_3 radiated by plates 1 and 2 as shown in Fig. 4. Taking into account that

$$I_{\text{in}} = I_1(z_2), \qquad (10)$$

$$I_{\text{out}} = I_2(z_2) + I_1(z_3) + I_2(z_3), \qquad (11)$$

we can obtain the integrodifferential equation for the temperature $T_2(t)$:

$$\alpha_2 \frac{dT_2(t)}{dt} = I_1(z_2, T_1) - I_2(z_2, T_2) - I_1(z_3, T_1) - I_2(z_3, T_2), \qquad (12)$$

where $\alpha_2 \equiv \rho_2 c_{v2} h_2$ and

$$I_i(z_j, T_i) = \int_0^\infty Q(\omega, z_j, T_i)\, d\omega, \qquad (13)$$

where $i = 1$ or 2, $j = 2$ or 3, and $Q(\omega, z_j, T_i)$ is the spectral intensity of thermal radiation from plate i at coordinate z_j and is calculated by Eq. (C1) (see Appendix C). Since the plates are in vacuum, then the coordinates z_j can be chosen by any means in such a way that they are topologically located as in Fig. 4.

It is necessary to note here that the set of Eqs. (12) implies that the spatial temperature distributions are homogeneous inside the plates. This condition is satisfied when the radiative heat transfer intensities $I_i(z_j, T_i)$ between plates are small enough compared with the heat transfer intensities inside the plates due to thermal conduction via heat carriers.

Before proceeding to describe the results of the simulations, we have to pay special attention to the condition of applicability of Eq. (12). Let us compare the radiative heat transfer intensity between plates, I_r, and the heat transfer intensity inside the plates due to thermal conduction via heat carriers, I_c. It can be seen from Figs. 1 and 2 that the intensity of the radiative heat transfer which is induced by a temperature difference of 300 K between plates can be roughly approximated by a simple formula:

$$I_r(h,d) \approx \begin{cases} 10^8/d^2 & \text{if } d < 10^4 \text{ nm} \\ \sqrt{h}/10 & \text{if } d \geqslant 10^4 \text{ nm} \end{cases}, \qquad (14)$$

where gap size d and thickness of plates h are expressed in nanometers. The heat transfer intensity inside a plate due to thermal conduction via heat carriers is found by the following formula:

$$I_c \approx \kappa \frac{\Delta T}{h}, \qquad (15)$$

where $\kappa = 3.6 \times 10^3$ W m^{-1} K^{-1} is the thermal conductivity of SiC and ΔT is also assumed to be 300 K. The condition of applicability of Eq. (12) is the following: $I_c \gg I_r$. This inequality ensures that the energy fluxes supported by heat carrier motion inside the plates are large enough to treat the spatial temperature distribution of the plates as homogeneous. After some arithmetic calculations we obtain

$$\begin{aligned} h &\ll 10^7 d^2 \quad \text{if} \quad d < 10^4 \text{ nm} \\ h &\ll 10^{32/3} \quad \text{if} \quad d \geqslant 10^4 \text{ nm}. \end{aligned} \qquad (16)$$

This condition is well satisfied in the rectangle $(h,d) : \{0 \leqslant h \leqslant 10^6 \text{ nm}\} \cup \{0 \leqslant d \leqslant 10^6 \text{ nm}\}$. Thus, in order to make sure that Eq. (12) can be used for simulation of the temperature dynamics in the the system of SiC plates, we consider only those values of parameters d and h that fall within this rectangle.

B. Results of simulations

Let us now simulate the time evolution of the temperature of the system of two parallel plates of SiC. We assume that the temperature of plate 1, $T_1(t)$, is constant and equals 300 K while the temperature of plate 2, $T_2(t)$, changes in time until the stationary state is established. The initial value of the temperature of plate 2 is denoted as $T_2(0)$. Our goal is to analyze the behavior of the function $T_2(t)$ for different $T_2(0)$, thicknesses of plates, d, and separation distances between plates, h. In calculations, the temperature dependence of the mass heat capacity of SiC is accounted for by the Debye model:

$$c_v(T) = \frac{9 n_a k N_A T^3}{\mu \theta_D^3} \int_0^{\theta_D/T} \frac{x^4 e^x}{(e^x - 1)^2} dx, \qquad (17)$$

where θ_D is the Debye temperature of SiC and is equal to 1200 K, μ is the molar mass of SiC and is equal to 40.1 g/mol, n_a is the number of atoms per unit cell and equals 2 for SiC, k is the Boltzmann constant, and N_A is the Avogadro constant. The mass density of SiC is 3.21 g/cm^3. The temperature dependencies of the density, refractive index, and extinction coefficient of SiC are neglected.

In order to find the temperature of plate 2 as a function of time, $T_2(t)$, we solve the integrodifferential equation in the set of Eqs. (12) which refers to plate 2 ($i = 2$) taking into account the initial condition $T_2(0)$. The solution $T_2(t)$ was found numerically using the Matlab function ode23tb.

The time evolutions $T_2(t)$ are shown in Fig. 5 in logarithmic time scale for thickness of plates $d = 100$ nm and an initial temperature of the absorbing plate $T_2(0) = 273$ K for various interplate distances. It can be seen from Fig. 5 that for small separation distances $d = 1$, 10, or 100 nm the temperature of plate 2 increases and tends to 300 K. In the case of $d = 1$ μm, temperature $T_2(t)$ increases; however, it does not reach the temperature of the heat source. This is explained by the fact that the heat transfer from plate 1 to plate 2 is so small that it cannot compensate the decrease of the internal energy of plate 2 due to its thermal emission. With increase of the separation distance d, the heat transfer intensity becomes smaller and smaller. At 2.7 μm the temperature T_2 does not change in time, and at $d < 2.7$ μm the temperature of plate 2 decreases. The temperature of plate 2 in stationary state, T_2^{SS}, is determined
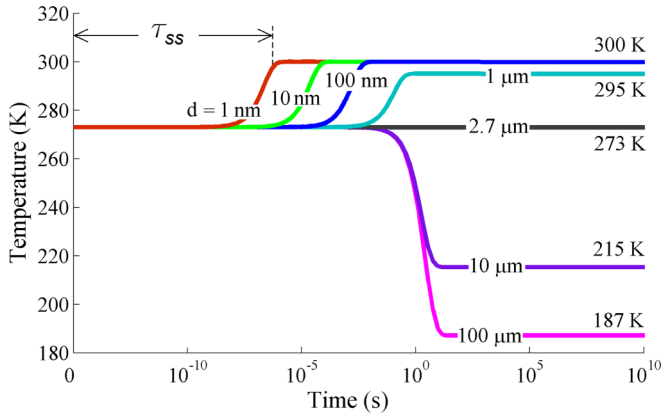
FIG. 5. (Color online) Time evolutions of the temperature of plate 2 calculated for different distances between plates. The thickness of the plates is $h = 100$ nm. The initial temperature of plate 2 is 273 K. $T_1 = 300$ K.

by the energy balance equation for the stationary state:

$$I_2\left(z_3, T_2^{SS}\right) + I_2\left(z_2, T_2^{SS}\right) = I_1(z_2, T_1) - I_1(z_3, T_1), \quad (18)$$

where the following notation is used: $T_2^{SS} \equiv \lim_{t \to \infty} T_2(t)$. The left side of Eq. (18) is the energy which is emitted by plate 2, while the right side is the energy which is absorbed in plate 2.

The physical process contained in Fig. 5 can be explained as follows. The thermal emission from plate 1 is absorbed by plate 2, resulting in change of temperature of plate 2. The change of temperature of plate 2 leads to the change of energy loss in plate 2 due to its emission. When thermal radiation from plate 2 becomes equal to its absorption of radiation from plate 1, the temperature $T_2(t)$ begins to be stationary.

Figure 6 represents the time evolutions $T_2(t)$ calculated for the initial temperatures $T_2(0) = 50, 300$, and 550 K and for two separation distances $d = 100$ nm and $100\ \mu$m. It can be seen
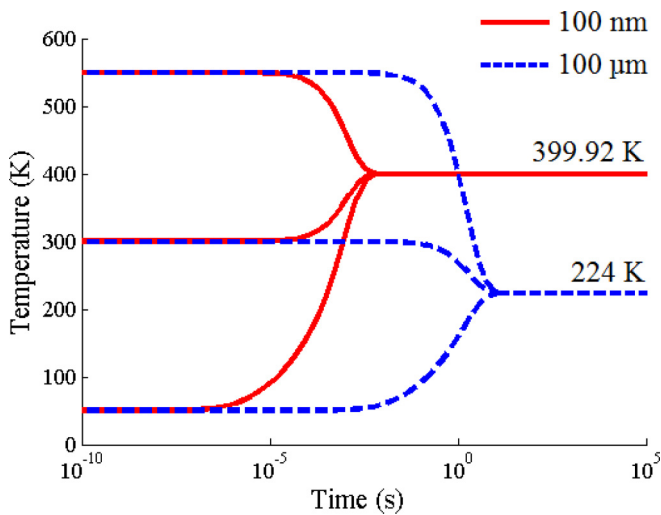

FIG. 6. (Color online) Time evolutions of the temperature of plate 2 calculated for distances between plates $d = 100$ nm and $100\ \mu$m and different initial conditions $T_2(0)$. The thickness of the plates is $h = 100$ nm. $T_1 = 400$ K.

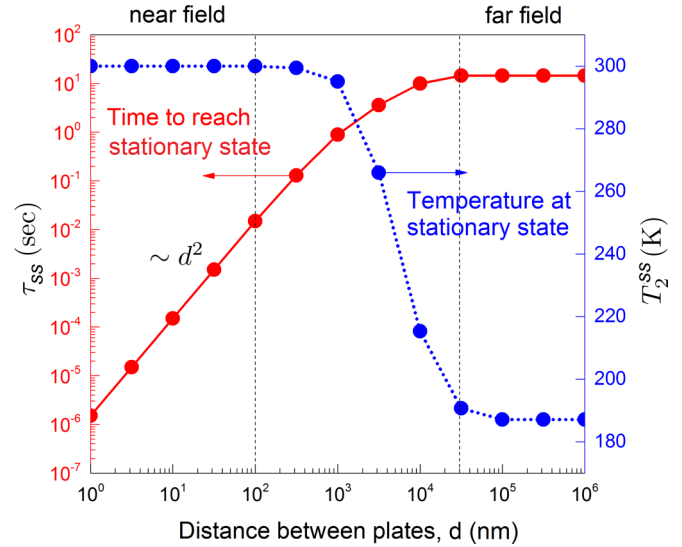FIG. 7. (Color online) Time it takes for plate 2 to reach stationary state, τ_{SS}, and temperature of plate 2 at stationary state, T_2^{SS}, as a function of the distance between plates. The thickness of the plates is $h = 100$ nm. $T_1 = 300$ K.

from Fig. 6 that the time it takes for plate 2 to reach stationary state does not appreciably depend on the initial temperature. Furthermore, as can be seen from Fig. 6, the initial temperature $T_2(0)$ does not influence the temperature of plate 2 in stationary state. This is in agreement with Eq. (18), which says that the temperature of plate 2 at stationary state depends only on the geometrical configuration of the structure, complex dielectric permittivity of the material, and temperature of the heat source. One can see from Fig. 5 that the time it takes for plate 2 to reach stationary state, τ_{SS}, increases with increase of the gap size.

Figure 7 shows the dependence of τ_{SS} and T^{SS} from d. When the distance between plates is $d < 100$ nm (near field), the time to reach stationary state is relatively short and increases as d^2 increases and the temperature T_2 reaches 300 K. The value of the parameter τ_{SS} changes from 1.5 μs to ≈ 15 ms when the distance d increases from 1 to 100 nm. In the far-field limit ($d > 30\ \mu$m) $\tau_{SS} = 14.5$ s and $T_2^{SS} = 187$ K, and these parameters do not depend on the gap size. In order to explain the characters of dependencies $T_2^{SS}(d)$ and $\tau_{SS}(d)$ in the near-field and far-field regimes, let us turn to Eq. (9). The right-hand side of this equation can be represented as the difference between the intensity of heat transfer from plate 1 to plate 2, $I_{12} = I_1(z_2, T_1) - I_1(z_3, T_1)$, and the intensity of thermal radiation emitted by plate 2, $I_{2,\text{rad}} = I_2(z_2, T_2) + I_2(z_3, T_2)$. As it was demonstrated in Figs. 1 and 2, in the near field, I_{12} is proportional to d^{-2} and approximately independent on h, so that we can write

$$I_{12} = \frac{1}{d^2} \times f_1(T_1), \quad (19)$$

where $f_1(T_1)$ is a function of the temperature of plate 1. Equation (19) assumes that the dependence of the heat transfer intensity I_{12} on d is the same for all temperatures T_1 in the temperature range under consideration. Our further simulations [52] of $I_{12}(d, h, T_1)$, which were made for different temperatures T_1, have shown that this assumption is indeed
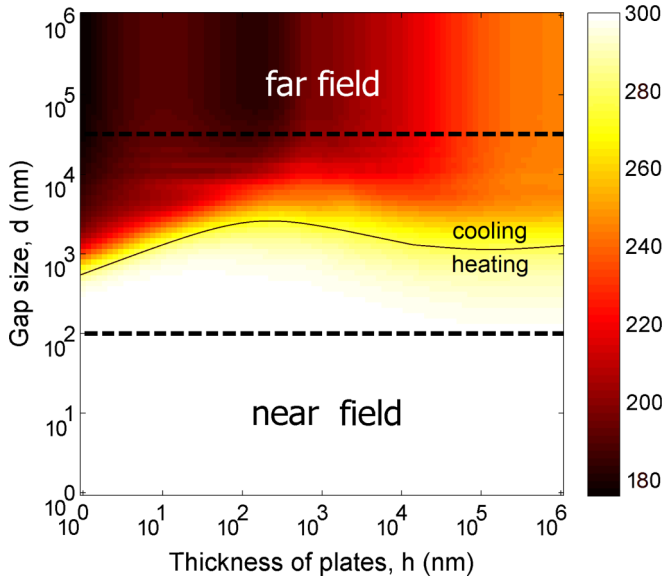
FIG. 8. (Color online) Temperature of plate 2 at stationary state as a two-dimensional function of the distance between plates, d, and thickness of the plates, h. The near-field and far-field regimes are separated by black dashed lines. The color scale on the right shows the calculated values of parameter T_2^{SS}. The solid line is a contour line at $T_2^{SS} = 273$ K and separates heating and cooling regimes in the assumption that $T_2(0) = 273$ K. $T_1 = 300$ K.
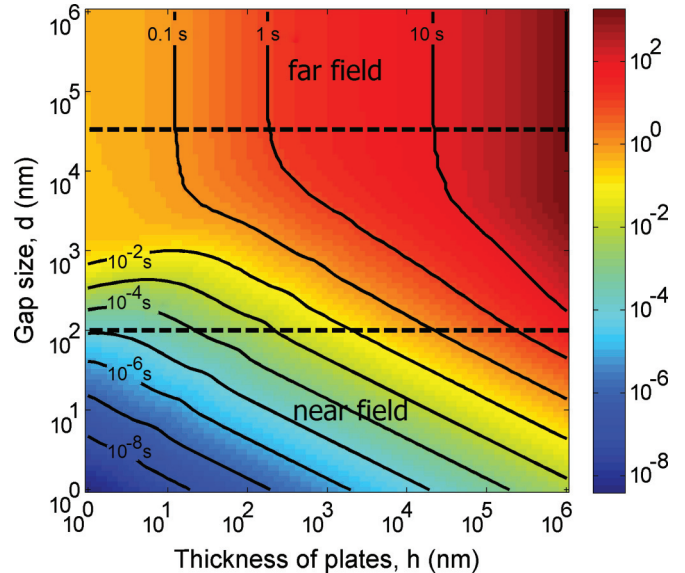

FIG. 9. (Color online) Time it takes for plate 2 to reach stationary state as a two-dimensional function of the distance between plates, d, and thickness of the plates, h. The contour lines are shown by black solid lines. The near-field and far-field regimes are separated by black dashed lines. The color scale on the right shows the calculated values of the parameter τ in seconds.

valid. As for the term $I_{2,\mathrm{rad}}$, the coupling between plates is dominant compared to the out-coupling to the outer space, so that $I_2(z_3, T_2) \ll I_2(z_2, T_2)$. Taking into account that $I_2(z_2, T_2) \sim d^{-2}$ one can rewrite the term $I_{2,\mathrm{rad}}$ as

$$I_{2,\mathrm{rad}} = \frac{1}{d^2} \times f_2[T_2(t)], \qquad (20)$$

where $f_2[T_2(t)]$ is a function of temperature of plate 2. Based on Eqs. (19) and (20) one can rewrite Eq. (9) as

$$\rho_2 c_{v2} h_2 \frac{dT(t)}{dt} = \frac{1}{d^2}[f_1(T_1) - f_2(T_2)], \qquad (21)$$

which gives the expression for the time it takes for plate 2 to reach stationary state in the near-field regime:

$$\tau_{SS}^{NF} = F(T_1, T_2(\tau_{SS})) \times \rho c_v h d^2. \qquad (22)$$

Similarly, we can find the expression for the time it takes for plate 2 to reach stationary state in the far-field regime:

$$\tau_{SS}^{FF} = F(T_1, T_2(\tau_{SS})) \times \rho c_v f(h), \qquad (23)$$

where $f(h)$ is some function of h reflecting the fact that in the far field the heat transfer intensity depends on h (see Fig. 2) and does not depend on d. Equations (22) and (23) explain the dependence $\tau_{SS}(d)$ shown in Fig. 7.

Let us now calculate the parameters T_2^{SS} and τ_{SS} as two-dimensional functions of the separation distance d and the thickness of plates h (see Figs. 8 and 9). When the separation distance is small enough (near field), the heat transfer intensity I_{12} is high and the temperature of plate 2 reaches the value of 300 K (see Fig. 8), and the time it takes for plate 2 to reach stationary state changes as hd^2 changes, in accordance with Eq. (22). In contrast to the near field, in the far field only

propagating waves contribute to the heat transfer from plate 1 to plate 2. In this case, the heat transfer from plate 1 to plate 2 cannot compensate the thermal radiation losses in plate 2 and the temperature of plate 2 in stationary state is less than the temperature of the heat source. The parameter τ_{SS} is constant over distance d and only depends on h. The character of this dependence is determined by the function $f(h)$ introduced in Eq. (23). In Fig. 8, the solid line shows the pairs (h,d) where $T_2^{SS} = T_2(0) = 273$ K. This line represents the threshold interplate distance which separates the heating and cooling regimes under the condition that the initial temperature of plate 2 is 273 K. The value of the threshold interplate distance ranges from 560 nm to 2.8 μm depending on the thickness between plates.

IV. CONCLUSION

Using the method of fluctuational electrodynamics in conjunction with the scattering matrix formalism, we have simulated the propagation of thermal radiation in a multilayer structure with SiC. We have shown that for a two-plate configuration the intensity of radiative heat exchange is mainly determined by the vacuum distance between plates while the thickness of plates does not play a crucial role. This affects the characteristics of the time evolution of the temperature of the sink plate. When the separation distance is small (the near-field regime), the time it takes for the sink plate to reach stationary state τ_{SS} is proportional to hd^2 and the temperature of the sink plate reaches the temperature of the heat source plate. When the separation distance is large (the far-field regime), τ_{SS} does not depend on d and the temperature at the stationary state of the sink plate is less than the temperature of the source plate. Although we have considered heat transfer dynamics of an

idealized two-plate configuration, our study reveals the most basic radiative interaction characteristics between two bodies in vacuum space. The conclusions as well as the method of simulation of time evolutions can be applied to understand heat transfer dynamics in more complicated planar structures other than the described system of two SiC plates. We believe that the results of this work can be useful for design of more complex systems where radiative heating is important, such as designs of absorbers and emitters in solar thermophotovoltaic devices.

APPENDIX A: SCATTERING MATRIX FORMALISM

The scattering matrix method is a very elegant tool for simulation of the propagation of plane waves and its analog for evanescent waves in the layered structure. The system under consideration (see Fig. 10) consists of N parallel layers placed between two semi-infinite media. All the layers are assumed to be isotropic and homogeneous. Thicknesses of the layers d_j ($j = 1, 2, \ldots, N$), their refractive indices, and extinction coefficients $\tilde{n}_i = n_j + ik_j$ are given.

Let us consider complex amplitudes of electric field, $E^+(z)$ and $E^-(z)$, of the plane waves propagating in a layered structure along positive and negative z directions at coordinate z. We would like to find the relation between the amplitudes $E^+(z)$ and $E^-(z)$ taken at two arbitrarily selected coordinates z' and z''. We find this relation in the following form:

$$\begin{bmatrix} E^+(z'') \\ E^-(z') \end{bmatrix} = \mathbb{S}(z',z'') \begin{bmatrix} E^+(z') \\ E^-(z'') \end{bmatrix}, \tag{A1}$$
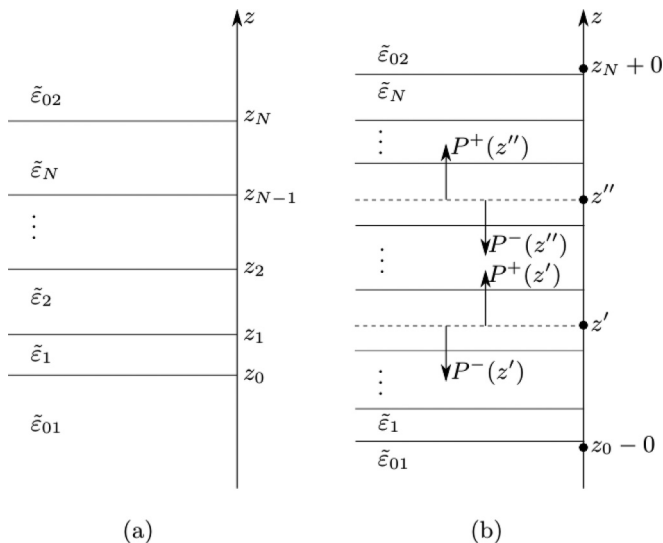

FIG. 10. (a) Sketch of the layered structure and (b) amplitudes of forward and backward traveling plane waves in the layered structure.

where the matrix $\mathbb{S}(z',z'')$ is called the *scattering matrix*. The column on the left-hand side describes the outgoing amplitudes to the layered substructure, defined by the coordinates z' and z'', while the column on the right-hand side stands for the incoming amplitudes. The matrix $\mathbb{S}^{\text{tot}} \equiv \mathbb{S}(z_0 - 0, z_N + 0)$ which connects the vectors of amplitudes taken at immediately opposite sides of the whole layered structure is called the *total scattering matrix*. Here we used the notation $z \pm 0 = \lim_{\Delta \to 0} (z \pm \Delta)$.

The procedure of calculation of the scattering matrix between two z coordinates is described in many publications [46,47,53,54]. The scattering matrix $\mathbb{S}(z',z'')$ is found iteratively, starting from the obvious equality:

$$\mathbb{S}(z',z') = \mathbb{I}, \tag{A2}$$

where $\mathbb{I} \equiv \begin{bmatrix} 1 & 0 \\ 0 & 1 \end{bmatrix}$. At each iteration step we find the new matrix $\mathbb{S}^{**} \equiv \mathbb{S}(z',z^{**})$ from the matrix $\mathbb{S}^* \equiv \mathbb{S}(z',z^*)$ calculated in the previous iteration step. If both points z^{**} and z^* lie in layer j then the elements of the matrices $\mathbb{S}^{**}$ and $\mathbb{S}^*$ are related as

$$\mathbb{S}_{11}^{**} = \mathbb{S}_{11}^* e^{ik_z L}, \tag{A3a}$$

$$\mathbb{S}_{12}^{**} = \mathbb{S}_{12}^* e^{2ik_z L}, \tag{A3b}$$

$$\mathbb{S}_{21}^{**} = \mathbb{S}_{21}^*, \tag{A3c}$$

$$\mathbb{S}_{22}^{**} = \mathbb{S}_{22}^* e^{ik_z L}, \tag{A3d}$$

where $\tilde{\varepsilon}_i \equiv \tilde{n}_i^2$, $k_z = \pm\sqrt{\left(\frac{\omega}{c}\right)^2 \tilde{\varepsilon}_j - k_x^2}$ is the z component of the wave vector of the propagating light in layer j and $L = z^{**} - z^*$. The negative sign of the square root is chosen when $\arg(\tilde{\varepsilon}_i) > \pi$ (see [55]). If the coordinates z^{**} and z^* lie at immediately opposite sides of an interface z_j, i.e., $z^{**} = z_j + 0$ and $z^* = z_j - 0$ [56], then the relation between matrices $\mathbb{S}^{**}$ and $\mathbb{S}^*$ can be found from the boundary conditions for the electric field and has the following form:

$$\mathbb{S}_{11}^{**} = \frac{\mathbb{S}_{11}^* t}{1 - \mathbb{S}_{12}^* r}, \tag{A4a}$$

$$\mathbb{S}_{12}^{**} = \frac{\mathbb{S}_{12}^* - r}{1 - \mathbb{S}_{12}^* r}, \tag{A4b}$$

$$\mathbb{S}_{21}^{**} = \frac{\mathbb{S}_{11}^{**} \mathbb{S}_{22}^* r}{t} + \mathbb{S}_{21}^*, \tag{A4c}$$

$$\mathbb{S}_{22}^{**} = \frac{\mathbb{S}_{22}^* (r \mathbb{S}_{12}^{**} + 1)}{t}, \tag{A4d}$$

where r and t are the Fresnel coefficients of the jth interface. Therefore the calculation of the total scattering matrix of the whole structure, $\mathbb{S}_{\text{tot}}$, can be performed by the following sequence of iterations:

$$\mathbb{S}(z_0 - 0, z_0 - 0) \longrightarrow \mathbb{S}(z_0 - 0, z_0 + 0) \longrightarrow$$
$$\longrightarrow \mathbb{S}(z_0 - 0, z_1 - 0) \longrightarrow \mathbb{S}(z_0 - 0, z_1 + 0) \longrightarrow$$
$$\longrightarrow \mathbb{S}(z_0 - 0, z_2 - 0) \longrightarrow \mathbb{S}(z_0 - 0, z_2 + 0) \longrightarrow \cdots$$
$$\longrightarrow \mathbb{S}(z_0 - 0, z_N - 0) \longrightarrow \mathbb{S}(z_0 - 0, z_N + 0).$$

Knowledge of the total scattering matrix of a structure enables us to determine the reflection, transmission, and

absorption coefficient of the layered structure at a given frequency ω:

$$R \equiv |r|^2 = |\mathbb{S}_{21}^{\text{tot}}|^2, \tag{A5a}$$

$$T \equiv |t|^2 = \frac{\text{Re}[k_z(z_N + 0)]}{\text{Re}[k_z(z_0 - 0)]} |\mathbb{S}_{11}^{\text{tot}}|^2, \tag{A5b}$$

$$A = 1 - R - T. \tag{A5c}$$

The aforementioned algorithm for calculation of the scattering matrix $\mathbb{S}(z',z'')$ between two arbitrary coordinates z' and z'' in an arbitrary layered structure is used in simulation of the radiative heat propagation in the multilayer structure.

APPENDIX B: METHOD OF SOURCE TERMS FOR DIPOLE EMISSION

Using the scattering matrix formalism one can simulate the electromagnetic field of emission of dipoles located in an arbitrary layered structure. The corresponding algorithm is described as a method of source terms for dipole emission and is well described in [57].

Let us consider a layered system with a plane of oscillating electrical dipoles (see Fig. 11). The plane is assumed to be parallel to the layer interfaces, to be located in layer s and to have coordinate z_s. We aim to calculate the components of electric and magnetic fields at coordinate z_c at a given frequency of emitted light ω, the x component of the wave vector k_x, and a given polarization. From the boundary conditions for the tangential components of the electric and magnetic vectors, one can obtain the following relation between the complex amplitudes of waves lying immediately on opposite sides of the plane with oscillating dipoles [57,58]:

$$E^+(z_s - 0) = E^+(z_s + 0) - J^+ \tag{B1}$$
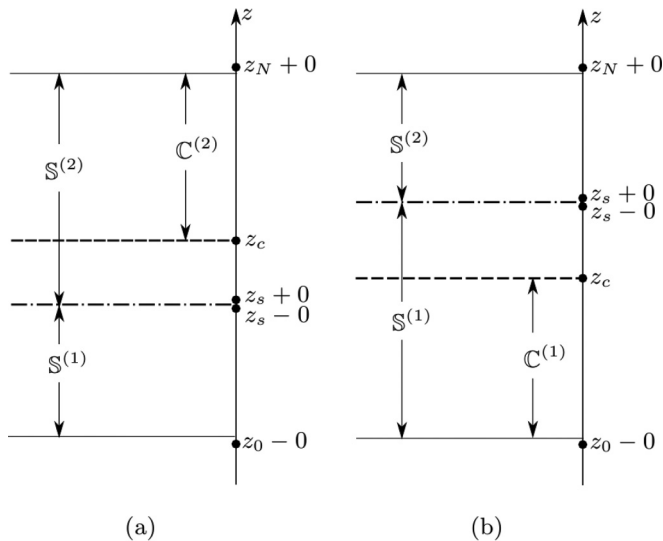$$E^-(z_s - 0) = E^-(z_s + 0) - J^-,$$

FIG. 11. Sketch of the layered structure with a plane of oscillating dipoles for the case (a) $z_c > z_s$ and (b) $z_c < z_s$. The plane of oscillating dipoles is denoted by the dash-dotted line.

where for horizontal chaotically oriented dipoles

$$J^\pm = \begin{cases} \mp\sqrt{\frac{3}{16\pi}} & \text{in } s \text{ polarization} \\ -\frac{k_{zs}}{k_s}\sqrt{\frac{3}{16\pi}} & \text{in } p \text{ polarization} \end{cases} \tag{B2}$$

and for vertical dipoles

$$J^\pm = \begin{cases} 0 & \text{in } s \text{ polarization} \\ \mp\frac{k_x}{k_s}\sqrt{\frac{3}{8\pi}} & \text{in } p \text{ polarization} \end{cases}. \tag{B3}$$

In Eqs. (B2) and (B3) the z component of wave vector k_{zs} is calculated for layer s and $k_s = \omega\tilde{n}_s/c$, where $\tilde{n}_s$ is the refractive index of layer s. The amplitudes of positive and negative traveling plane waves $E^\pm$ taken at coordinates $z = 0 - 0, z_s \pm 0$, and z_N are related by scattering matrices $\mathbb{S}^{(1)}$ and $\mathbb{S}^{(2)}$:

$$\begin{bmatrix} 0 \\ E^-(z_s - 0) \end{bmatrix} = \mathbb{S}^{(1)} \begin{bmatrix} E^+(z_s - 0) \\ E^-(0 - 0) \end{bmatrix}$$
$$\begin{bmatrix} E^+(z_N + 0) \\ E^-(z_s + 0) \end{bmatrix} = \mathbb{S}^{(2)} \begin{bmatrix} E^+(z_s + 0) \\ 0 \end{bmatrix}. \tag{B4}$$

The zero components in the 1×2 vectors reflect the fact that there is no incident plane wave either on the top or bottom of the sample. Taking into account Eqs. (B1) and (B4) one can find the expression for the amplitudes of waves out-coupled from the structure:

$$E^+(z_N + 0) = \frac{+J^+ - \mathbb{S}_{12}^{(1)} J^-}{\mathbb{S}_{12}^{(1)} \mathbb{S}_{21}^{(2)} - 1} \times \mathbb{S}_{11}^{(2)},$$
$$E^-(0 - 0) = \frac{-J^- + \mathbb{S}_{21}^{(2)} J^+}{\mathbb{S}_{21}^{(2)} \mathbb{S}_{12}^{(1)} - 1} \times \mathbb{S}_{22}^{(1)}. \tag{B5}$$

After algebraic manipulations one can find the expressions for the amplitudes of waves at coordinate z_c. If $z_c > z_s$, then

$$E^+(z_c) = \frac{1}{\mathbb{C}_{11}^{(2)}} \times E^+(z_N + 0),$$
$$E^-(z_c) = \frac{\mathbb{C}_{21}^{(2)}}{\mathbb{C}_{11}^{(2)}} \times E^+(z_N + 0), \tag{B6}$$

where the matrix $\mathbb{C}^{(2)}$ connects the amplitudes at coordinates z_c and $z_N + 0$ [see Fig. 11(a)]. In the opposite case, when $z_c < z_s$, the amplitudes at z_c are given by

$$E^+(z_c) = \frac{\mathbb{C}_{12}^{(1)}}{\mathbb{C}_{22}^{(1)}} \times E^-(0 - 0),$$
$$E^-(z_c) = \frac{1}{\mathbb{C}_{22}^{(1)}} \times E^-(0 - 0), \tag{B7}$$

and the matrix $\mathbb{C}^{(1)}$ connects the amplitudes at coordinates $z = 0 - 0$ and z_c [see Fig. 11(b)].

The vector of the electric field at coordinate z_c is expressed as

$$\vec{E}(z_c) = E^+(z_c)\vec{p}_+ + E^-(z_c)\vec{p}_-, \tag{B8}$$

where

$$\vec{p}_\pm = \begin{cases} \{0,1,0\} & \text{in } s \text{ polarization} \\ \{\pm\frac{k_{zc}}{k_c}, 0, \mp\frac{k_x}{k_c}\} & \text{in } p \text{ polarization} \end{cases}. \tag{B9}$$

The vector of the magnetic field is calculated and given by

$$\vec{H}(z_c) = \sqrt{\varepsilon_c}E^+(z_c)[\vec{k}_+ \times \vec{p}_+] + \sqrt{\varepsilon_c}E^-(z_c)[\vec{k}_- \times \vec{p}_-],$$
(B10)

where $\vec{k}_{\pm} = [\vec{p}_{\pm}^{(p)} \times \vec{p}_{\pm}^{(s)}]$. The Poynting vector at an arbitrary coordinate z_c is calculated as

$$\vec{S}(z_c) = \frac{c}{4\pi}\mathrm{Re}[\vec{E}(z_c) \times \vec{H}(z_c)].$$
(B11)

The intensity of dipole emission which emerges in the structure can be found via the z component of the pointing vector:

$$I_{\mathrm{out}} = \frac{n_0 k_{z0}^2}{n_s k_{zs}^2} \times S_z(z_N + 0).$$
(B12)

In Eq. (B12) the factor $n_0 k_{z0}^2/n_s k_{zs}^2$ is used to account for the change in solid angle that is due to refraction for plane waves or its analog for evanescent waves [57].

It is worth noting that the described method is a powerful tool for simulation of interference effects in the luminescence spectra of the samples where one or several layers can emit light (see, for example, [59–62]).

APPENDIX C: INTENSITY OF THERMAL RADIATION

Let us consider a problem of calculation of the thermal emission of a source layer into a multilayered structure. We are going to find the z component of the energy flux at an arbitrary coordinate z_c of the electromagnetic waves thermally radiated by a source layer in an arbitrary layered structure at a given temperature of the source layer, T, and frequency, ω.

The mathematical model for the calculation of the radiative heat flux is well described in literature (see, for example, [3,20]). The thermal radiation is described as a fluctuating electromagnetic field generated by chaotic motion of charged particles inside the body. Using the Green's-function formalism, one can express the electric and magnetic fields at coordinate z due to the oscillating dipole at coordinate z' via the vector of the current density of this dipole [see Eq. (2)]. At the same time, the fluctuation-dissipation theorem Eq. (4) connects the ensemble average of the spatial correlation function of current density and the mean energy of Planck's oscillator. Using the expression of spectral intensity of thermal radiation, Eq. (5), and representing the dyadic Green's functions G^E and G^H in a plane-wave form [20], we obtain the following expression for the spectral intensity of thermal radiation at coordinate z due to the emission by the source:

$$Q(\omega,z,T) = \frac{\omega^2 \Theta(\omega,T)}{\pi^2 c^2}$$
$$\times \mathrm{Re}\left[i\varepsilon_s'' \int_0^\infty k_x dk_x \int_{z_s}^{z_s+h} dz' q(\omega,k_x,z,z')\right],$$
(C1)

where coordinates z_s and $z_s + h$ confine the emitting layer, h is the thickness of the emitting layer, and

$$q(\omega,k_x,z,z') \equiv g_{x\alpha}^E(\omega,k_x,z,z')g_{y\alpha}^{H*}(\omega,k_x,z,z')$$
$$- g_{y\alpha}^E(\omega,k_x,z,z')g_{x\alpha}^{H*}(\omega,k_x,z,z'). \quad (C2)$$

Parameter ε_s'' is the imaginary part of the relative permittivity of the source layer, $g_{i,k}^E$ and $g_{i,k}^H$ are the Weyl components of the dyadic Green's functions, and $\Theta(\omega,T) = \hbar\omega/(\exp \hbar\omega/k_B T - 1)$ is the mean energy of a harmonic oscillator. In order to calculate the intensity of thermal radiation at coordinate z one has to integrate the spectral intensity of thermal radiation $Q(\omega,z,T)$ over the frequency:

$$I(z,T) = \int_0^\infty Q(\omega,z,T)d\omega.$$
(C3)

The Weyl components of the dyadic Green's functions can be written in tensor form as [20]

$$g^E(k_x,z,z') = \begin{bmatrix} g_{xx}^E & 0 & g_{xz}^E \\ 0 & g_{yy}^E & 0 \\ g_{zx}^E & 0 & g_{zz}^E \end{bmatrix},$$
(C4a)

$$g^H(k_x,z,z') = \begin{bmatrix} 0 & g_{xy}^H & 0 \\ g_{yx}^H & 0 & g_{yz}^H \\ 0 & g_{zy}^H & 0 \end{bmatrix}.$$
(C4b)

It can be shown [19,20] that the elements of the g^E tensor are

$$g_{xx}^E = (+A_p - B_p - C_p + D_p)\frac{ik_{zc}}{2k_s k_c},$$
(C5a)

$$g_{xz}^E = (-A_p + B_p - C_p + D_p)\frac{ik_{zc}k_x}{2k_{zs}k_s k_c},$$
(C5b)

$$g_{yy}^E = (+A_s + B_s + C_s + D_s)\frac{i}{2k_{zs}},$$
(C5c)

$$g_{zx}^E = (-A_p - B_p + C_p + D_p)\frac{ik_x}{2k_s k_c},$$
(C5d)

$$g_{zz}^E = (+A_p + B_p + C_p + D_p)\frac{ik_x^2}{2k_{zs}k_s k_c},$$
(C5e)

and the elements of the g^H tensor are

$$g_{xy}^H = (+A_s - B_s + C_s - D_s)\frac{k_{zc}}{2k_s},$$
(C6a)

$$g_{yx}^H = (-A_p - B_p + C_p + D_p)\frac{k_c}{2k_s},$$
(C6b)

$$g_{yz}^H = (+A_p + B_p + C_p + D_p)\frac{k_c k_x}{2k_s k_{zs}},$$
(C6c)

$$g_{zy}^H = (-A_s - B_s - C_s - D_s)\frac{k_x}{2k_{zs}}.$$
(C6d)

The subscripts s and p denote different polarizations of light. k_s and k_c are the wave vectors in the source and sink layers correspondingly. The coefficients $A(k_x,z,z')$ and $B(k_x,z,z')$ are the amplitudes of forward and backward traveling plane waves at a coordinate z due to emission of plane waves of unit amplitude in layer s at coordinate z' in the *positive z* direction. Likewise, the coefficients A, B, C, and D are the amplitudes of forward and backward traveling plane waves at a coordinate z due to the emission of a plane wave of unit amplitude in layer s at coordinate z' in the *negative z* direction. The coefficients A, B, C, and D can be expressed in terms of the scattering matrices connecting the different z coordinates in the structure. The scattering matrix method
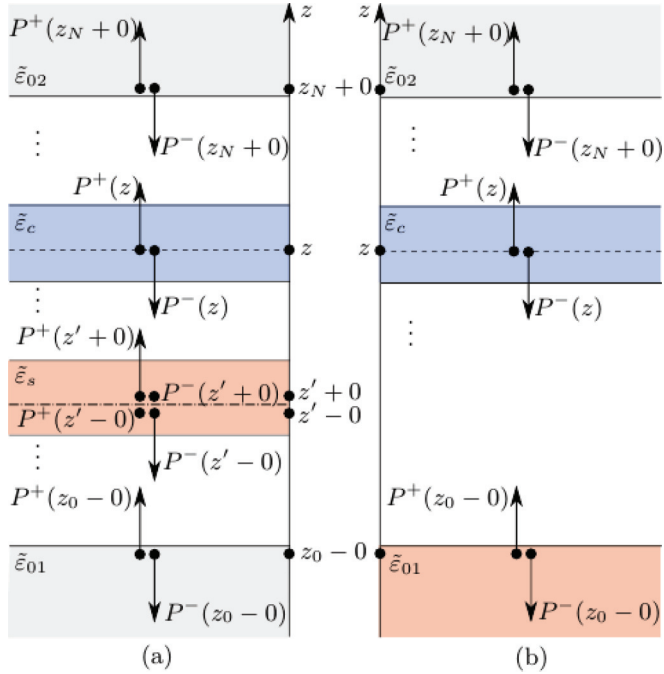
FIG. 12. (Color online) Layered structures with a source layer (pink) and receiver layer (blue). Arrows show the complex amplitudes of forward and backward traveling plane waves taken at specific coordinates. Amplitudes $P^+(z'-0)$ and $P^-(z'+0)$ in panel (a) are shown by dots in order to avoid overlapping with arrows labeled as $P^+(z'+0)$ and $P^-(z'-0)$.

allows us to find these coefficients for any arbitrary layered structure and for any arbitrary position of the source, z', and the point z where the radiative radiative heat flux is calculated.

Let us consider the most general case when $z_0 < z' < z < z_N$ [see Fig. 12(a)]. It can be shown (see Appendix A) that

the coefficients A, B, C, and D have the following explicit expressions:

$$A = \frac{\mathbb{S}''_{11}}{\mathbb{C}''_{11}} \times \frac{1}{1 - \mathbb{S}'_{12}\mathbb{S}''_{21}}, \tag{C7a}$$

$$B = \mathbb{C}''_{21}A, \tag{C7b}$$

$$C = \mathbb{S}'_{12}A, \tag{C7c}$$

$$D = \mathbb{S}'_{12}\mathbb{C}''_{21}A, \tag{C7d}$$

where the following notations are used:

$$\mathbb{C}' \equiv \mathbb{S}(0,z), \tag{C8a}$$

$$\mathbb{S}' \equiv \mathbb{S}(0,z_s - 0), \tag{C8b}$$

$$\mathbb{C}'' \equiv \mathbb{S}(z,z_N + 0), \tag{C8c}$$

$$\mathbb{S}'' \equiv \mathbb{S}(z_s + 0,z_N + 0). \tag{C8d}$$

If $z_0 < z < z_s < z_N$ then Eqs. (C7) and (C8) are valid with the substitutions $\mathbb{C}' \leftrightarrow \mathbb{C}''$, $\mathbb{S}' \leftrightarrow \mathbb{S}''$, $1 \leftrightarrow 2$. The calculation procedure of the matrices $\mathbb{C}'$, $\mathbb{C}''$, $\mathbb{S}'$, and $\mathbb{S}''$ is explained in Appendix A. Equations (C7) describe the radiation from the one plane of chaotically oriented dipoles. In order to calculate the radiative heat flux from a layer of a certain thickness, one has to integrate the flux over the corresponding z coordinates. In numerical simulations the integration is often replaced by the summation of the heat fluxes calculated for different coordinates z'. This integration is introduced in Eq. (C1). In practice, the number of coordinates z' for summation depends not only on the emitting plate thickness but also on the separation distances between plates, so that the calculation time for the thick emitting plate and short separation distances might be very long. In order to avoid this problem here we give the explicit expression of the result of analytical integration over z' in Eq. (C1):

$$\int_{z_s}^{z_s+h} dz' q(\omega,k_x,z,z') = \frac{i}{2k'_{zs}}(1 - e^{-2ihk'_{zs}})(+A_sC_s^*\tau\psi^* + A_sD_s^*\tau\psi^* - B_sC_s^*\tau\psi^* - B_sD_s^*\tau\psi^* - A_pC_p^*\alpha\beta^* - B_pC_p^*\alpha\beta^*$$

$$+A_pD_p^*\alpha\beta^* + B_pD_p^*\alpha\beta^* + A_pC_p^*\gamma\delta^* + B_pC_p^*\gamma\delta^* - A_pD_p^*\gamma\delta^* - B_pD_p^*\gamma\delta^*)$$

$$-\frac{i}{2k'_{zs}}(1 - e^{+2ihk'_{zs}})(+A_pC_p^*\alpha\beta^* + A_pD_p^*\alpha\beta^* - B_pC_p^*\alpha\beta^* - B_pD_p^*\alpha\beta^* - A_pC_p^*\gamma\delta^* - A_pD_p^*\gamma\delta^*$$

$$+B_pC_p^*\gamma\delta^* + B_pD_p^*\gamma\delta^* - A_sC_s^*\tau\psi^* + A_sD_s^*\tau\psi^* - B_sC_s^*\tau\psi^* + B_sD_s^*\tau\psi^*)$$

$$-\frac{1}{2k''_{zs}}(1 - e^{+2hk''_{zs}})(+C_sD_s^*\tau\psi^* - C_sC_s^*\tau\psi^* - D_sC_s^*\tau\psi^* + D_sD_s^*\tau\psi^* - C_pC_p^*\alpha\beta^* - C_pD_p^*\alpha\beta^*$$

$$+D_pC_p^*\alpha\beta^* + D_pD_p^*\alpha\beta^* - C_pC_p^*\gamma\delta^* - C_pD_p^*\gamma\delta^* + D_pC_p^*\gamma\delta^* + D_pD_p^*\gamma\delta^*)$$

$$+\frac{1}{2k''_{zs}}(1 - e^{-2hk''_{zs}})(+A_pA_p^*\alpha\beta^* + A_pB_p^*\alpha\beta^* - B_pA_p^*\alpha\beta^* - B_pB_p^*\alpha\beta^* - B_pB_p^*\gamma\delta^* - B_pD_A^*\gamma\delta^*$$

$$+A_pB_p^*\gamma\delta^* + A_pA_p^*\gamma\delta^* + B_sA_s^*\tau\psi^* - B_sB_s^*\tau\psi^* - A_sB_s^*\tau\psi^* + A_sA_s^*\tau\psi^*), \tag{C9}$$

where

$$\alpha = \frac{ik_{zc}}{2k_sk_c}, \quad \beta = \frac{k_c}{2k_s}, \quad \gamma = \frac{ik_{zc}k_x}{2k_{zs}k_sk_c},$$

$$\delta = \frac{k_ck_x}{2k_sk_{zs}}, \quad \tau = \frac{i}{2k_{zs}}, \quad \psi = \frac{k_{zc}}{2k_s}, \tag{C10}$$

k'_{zs} and k''_{zs} are the real and imaginary parts of the z component of the wave vector of the emitting layer. Note that both k'_{zs} and k''_{zs} are positive. Coefficients A, B, C, and D are calculated by Eqs. (C7) for the coordinate z' closest to the receiving layer (i.e., for $z' = z_s + h$ when $z_s < z$ and $z' = z_s$ when $z_s > z$.) The analytical expressions for the radiative heat flux in the case of few-layered structures can be obtained and were analyzed in many publications [9,14,16,49].

The expression for the intensity of thermal radiation can be simplified when the emitting layer is a semi-infinite substrate [see Fig. 12(b)]. Of course, one can treat the substrate as an additional very thick layer and integrate the heat flux over this layer. At the same time, as is shown in [20], the integral over z' in Eq. (C1) can be expressed as

$$\int_{-\infty}^{z_0-0} dz' q(\omega, k_x, z, z') = \frac{1}{2k''_{zs}} q(\omega, k_x, z, z_0 - 0). \quad \text{(C11)}$$

This means that we can calculate the heat flux from the semi-infinite source layer considering only one emitting plane in it, namely, $z_0 - 0$. The expressions for the coefficients A–D are also simplified:

$$A = \frac{\mathbb{S}''_{11}}{\mathbb{C}''_{11}}, \quad \text{(C12a)}$$

$$B = \mathbb{C}''_{21} A, \quad \text{(C12b)}$$

$$C = 0, \quad \text{(C12c)}$$

$$D = 0. \quad \text{(C12d)}$$

The scattering matrices $\mathbb{C}'$ and $\mathbb{C}''$ are defined by Eqs. (C8a) and (C8c). The zero values of the coefficients C and D mean that the plane waves, which are emitted by dipoles in the lower semi-infinite media, do not contribute to the amplitudes at the coordinate z where the flux is calculated.

Let us consider the next very important case where the sink is a semi-infinite layer and the source is a layer of a certain thickness [see Fig. 13(a)]. The monochromatic radiative heat flux is calculated by Eq. (C1) with $z = z_N + 0$. Since the receiver is a semi-infinite medium, $\mathbb{C}'' = \mathbb{I}$ and the coefficients in the tensors $g^{E,H}$ are given by the following expressions:

$$A = \frac{\mathbb{S}''_{11}}{1 - \mathbb{S}'_{12}\mathbb{S}''_{21}}, \quad \text{(C13a)}$$

$$B = 0, \quad \text{(C13b)}$$

$$C = \mathbb{S}'_{12} A, \quad \text{(C13c)}$$
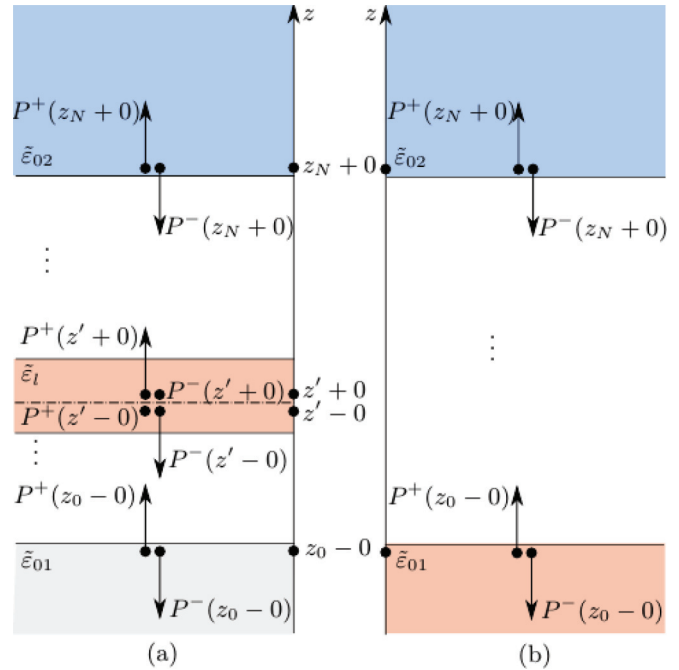
$$D = 0. \quad \text{(C13d)}$$

FIG. 13. (Color online) Layered structures with a source layer (pink) and receiver layer (blue). Arrows show the complex amplitudes of forward and backward traveling plane waves taken at specific coordinates. Amplitudes $A(z' - 0)$ and $B(z' + 0)$ in panel (a) are shown by dots in order to avoid overlapping with arrows labeled as $A(z' + 0)$ and $B(z' - 0)$.

Zero values of the coefficients B and D mean that there is no incident light on the structure from the upper semi-infinite medium.

Finally, when both the source plate and sink plate are as semi-infinite as is shown in Fig. 13(b), $\mathbb{C}'' = \mathbb{I}$, $\mathbb{S}' = \mathbb{I}$, and $\mathbb{S}'' = \mathbb{S}^{\text{tot}}$. Therefore, the integration over z' in Eq. (C1) is replaced by Eq. (C11) with the following expressions for the coefficients A, B, C, and D:

$$A = \mathbb{S}^{\text{tot}}_{11}, \quad \text{(C14a)}$$

$$B = 0, \quad \text{(C14b)}$$

$$C = 0, \quad \text{(C14c)}$$

$$D = 0. \quad \text{(C14d)}$$

The procedure of calculation of the total scattering matrix $\mathbb{S}^{\text{tot}}$ is described in Appendix A.

---

[1] S. M. Rytov, Sov. Phys. JETP **6**, 130 (1958).

[2] D. Polder and M. Van Hove, Phys. Rev. B **4**, 3303 (1971).

[3] K. Joulain, J.-P. Mulet, F. Marquier, R. Carminati, and J.-J. Greffet, Surface Science Reports **57**, 59 (2005).

[4] M. D. Whale and E. G. Cravalho, IEEE Trans. Energy Conversion **17**, 130 (2002).

[5] P. Greiff, R. Dimatteo, E. Brown, and C. Leitz, US Patent No. 20,130,092,212 (2013).

[6] M. Laroche, R. Carminati, and J.-J. Greffet, J. Appl. Phys. **100**, 063704 (2006).

[7] A. Narayanaswamy and G. Chen, Phys. Rev. B **70**, 125101 (2004).

[8] X. Liu, T. Tyler, T. Starr, A. F. Starr, N. M. Jokerst, and W. J. Padilla, Phys. Rev. Lett. **107**, 045901 (2011).

[9] S. Edalatpour and M. Francoeur, J. Quant. Spectrosc. Radiat. Transfer **118**, 75 (2013).

[10] J.-J. Greffet, R. Carminati, K. Joulain, J.-P. Mulet, S. Mainguy, and Y. Chen, Nature (London) **416**, 61 (2002).

[11] J. Drevillon and P. Ben-Abdallah, J. of Appl. Phys. **102**, 114305 (2007).

[12] B. J. Lee and Z. M. Zhang, J. Appl. Phys. **100**, 063529 (2006).

[13] W. A. Challener, C. Peng, A. Itagi, D. Karns, W. Peng, Y. Peng, X. Yang, X. Zhu, N. Gokemeijer, Y.-T. Hsia, *et al.*, Nature Photonics **3**, 220 (2009).

[14] P. Ben-Abdallah, K. Joulain, J. Drevillon, and G. Domingues, J. Appl. Phys. **106**, 044306 (2009).

[15] S.-A. Biehs, M. Tschikin, R. Messina, and P. Ben-Abdallah, Appl. Phys. Lett. **102**, 131106 (2013).

[16] A. I. Volokitin and B. N. J. Persson, Rev. Mod. Phys. **79**, 1291 (2007).

[17] S. Basu, Z. M. Zhang, and C. J. Fu, Int. J. Energy Res. **33**, 1203 (2009).

[18] M. Francoeur, M. P. Menguc, and R. Vaillon, Appl. Phys. Lett. **93**, 043109 (2008).

[19] M. Francoeur and M. Pinar Mengüç, J. Quant. Spectrosc. Radiat. Transfer **109**, 280 (2008).

[20] M. Francoeur, M. Pinar Mengüç, and R. Vaillon, J. Quant. Spectrosc. Radiat. Transfer **110**, 2002 (2009).

[21] M. Tschikin, P. Ben-Abdallah, and S.-A. Biehs, Phys. Lett. A **376**, 3462 (2012).

[22] B. Neuner III, C. Wu, G. Ten Eyck, M. Sinclair, I. Brener, and G. Shvets, Appl. Phys. Lett. **102**, 211111 (2013).

[23] M. De Zoysa, T. Asano, K. Mochizuki, A. Oskooi, T. Inoue, and S. Noda, Nature Photonics **6**, 535 (2012).

[24] B. Liu and S. Shen, Phys. Rev. B **87**, 115403 (2013).

[25] R. Guérout, J. Lussange, F. S. S. Rosa, J.-P. Hugonin, D. A. R. Dalvit, J.-J. Greffet, A. Lambrecht, and S. Reynaud, Phys. Rev. B **85**, 180301 (2012).

[26] A. Narayanaswamy and G. Chen, Phys. Rev. B **77**, 075125 (2008).

[27] R. S. Ottens, V. Quetschke, S. Wise, A. A. Alemi, R. Lundock, G. Mueller, D. H. Reitze, D. B. Tanner, and B. F. Whiting, Phys. Rev. Lett. **107**, 014301 (2011).

[28] S.-A. Biehs, E. Rousseau, J.-J. Greffet *et al.*, Phys. Rev. Lett. **105**, 234301 (2010).

[29] S. E. Han and D. J. Norris, Phys. Rev. Lett. **104**, 043901 (2010).

[30] G. Domingues, S. Volz, K. Joulain, and J.-J. Greffet, Phys. Rev. Lett. **94**, 085901 (2005).

[31] P. Ben-Abdallah and S.-A. Biehs, Phys. Rev. Lett. **112**, 044301 (2014).

[32] A. W. Rodriguez, O. Ilic, P. Bermel, I. Celanovic, J. D. Joannopoulos, M. Soljačić, and S. G. Johnson, Phys. Rev. Lett. **107**, 114302 (2011).

[33] K. Sasihithlu and A. Narayanaswamy, Phys. Rev. B **83**, 161406 (2011).

[34] C. Otey and S. Fan, Phys. Rev. B **84**, 245431 (2011).

[35] A. P. McCauley, M. T. H. Reid, M. Krüger, and S. G. Johnson, Phys. Rev. B **85**, 165104 (2012).

[36] R. Messina, M. Tschikin, S.-A. Biehs, and P. Ben-Abdallah, Phys. Rev. B **88**, 104307 (2013).

[37] V. Yannopapas and N. V. Vitanov, Phys. Rev. Lett. **110**, 044302 (2013).

[38] M. Tschikin, S.-A. Biehs, F. Rosa, and P. Ben-Abdallah, European Physical Journal B **85**, 1 (2012).

[39] V. Yannopapas, J. Phys. Chem. C **117**, 14183 (2013).

[40] S.-A. Biehs and G. S. Agarwal, J. Opt. Soc. Am. B **30**, 700 (2013).

[41] L. Zhu, C. R. Otey, and S. Fan, Phys. Rev. B **88**, 184301 (2013).

[42] M. Krüger, G. Bimonte, T. Emig, and M. Kardar, Phys. Rev. B **86**, 115423 (2012).

[43] R. Messina and M. Antezza, Europhysics Letters **95**, 61002 (2011).

[44] M. Krüger, T. Emig, and M. Kardar, Phys. Rev. Lett. **106**, 210404 (2011).

[45] R. Messina and M. Antezza, Phys. Rev. A **89**, 052104 (2014).

[46] D. Y. K. Ko and J. C. Inkson, Phys. Rev. B **38**, 9945 (1988).

[47] S. G. Tikhodeev, A. L. Yablonskii, E. A. Muljarov, N. A. Gippius, and T. Ishihara, Phys. Rev. B **66**, 045102 (2002).

[48] S. A. Dyakov, V. A. Tolmachev, E. V. Astrova, S. G. Tikhodeev, V. Y. Timoshenko, and T. S. Perova, Proceedings of SPIE **7521**, 75210G (2009).

[49] J.-P. Mulet, K. Joulain, R. Carminati, and J.-J. Greffet, Microscale Thermophysical Engineering **6**, 209 (2002).

[50] M. Francoeur, M. P. Mengüç, and R. Vaillon, Phys. Rev. B **84**, 075436 (2011).

[51] S. Basu and M. Francoeur, Appl. Phys. Lett. **99**, 143107 (2011).

[52] For the sake of space, results of these simulations are not shown in the article; however, they are very similar to those shown in Figs. 1 and 2.

[53] D. M. Whittaker and I. S. Culshaw, Phys. Rev. B **60**, 2610 (1999).

[54] L. C. Botten, N. A. Nicorovici, R. C. McPhedran, C. M. d. Sterke, and A. A. Asatryan, Phys. Rev. E **64**, 046603 (2001).

[55] J. Skaar, Opt. Lett. **31**, 3372 (2006).

[56] Here we use the following notation: $z \pm 0 \equiv \lim_{\Delta \to 0}(z \pm \Delta)$.

[57] H. Benisty, R. Stanley, and M. Mayer, J. Opt. Soc. Am. A **15**, 1192 (1998).

[58] S. A. Dyakov, T. S. Perova, M. C. Q., Y.-H. Xie, S. A. Cherevkov, and A. N. Baranov, J. Raman Spectrosc. **44**, 803 (2013).

[59] S. A. Dyakov, D. M. Zhigunov, A. Hartel, M. Zacharias, T. S. Perova, and V. Y. Timoshenko, Appl. Phys. Lett. **100**, 061908 (2012).

[60] A. Zelenina, S. A. Dyakov, D. Hiller, S. Gutsch, V. Trouillet, M. Bruns, S. Mirabella, P. Löper, L. López-Conesa, J. López-Vidrier, *et al.*, J. Appl. Phys. **114**, 184311 (2013).

[61] D. Hiller, A. Zelenina, S. Gutsch, S. A. Dyakov, L. López-Conesa, J. López-Vidrier, S. Estrade, F. Peiro, B. Garrido, J. Valenta, M. Korinek, F. Trojanek, P. Maly, M. Schnabel, C. Weiss, S. Janz, and M. Zacharias, J. Appl. Phys. **115**, 204301 (2014).

[62] M. Schnabel, P. Löper, M. Canino, S. A. Dyakov, M. Allegrezza, M. Bellettato, J. López-Vidrier, S. Hernández, C. Summonte, B. Garrido, P. R. Wilshaw, and S. Janz, Solid State Phenom. **205-206**, 480 (2013).